

Impacts of Loop Current Frontal Cyclonic Eddies and Wind Forcing on the 2010 Gulf of Mexico Oil Spill

Nan D. Walker,¹ Chet T. Pilley,¹ Vandana V. Raghunathan,¹ Eurico J. D'Sa,¹ Robert R. Leben,² Nicholas G. Hoffmann,² Peter J. Brickley,³ Patrice D. Coholan,³ Neha Sharma,³ Hans C. Graber,⁴ and Raymond E. Turner⁴

The 2010 *Deepwater Horizon* Gulf of Mexico oil spill, the largest in U.S. history, highlights the environmental risks inherent in deepwater drilling. These risks were mitigated by rapid access to real-time satellite measurements from passive (optical, IR) and active (synthetic aperture radar, altimetry) sensors. This study employed satellite data, in tandem with in situ current and wind measurements, to track surface oil and to better understand the causes for observed large-scale motions during the 84 day episode. The analysis revealed the merger of three cyclonic eddies along the Loop Current's (LC's) northern margin, ultimately forming a larger and more vigorous cyclonic eddy, measuring 280×130 km on 18 May. This larger cyclonic eddy, in tandem with a smaller anticyclonic eddy and a LC meander, controlled the motion of the oil/dispersant mixture into deepwater (maximum current speed of 2.25 m s^{-1}), tripling the area of surface oiling from 9623 to 33,575 km^2 . Two main events limited the flow of oil to the Florida Straits, the accumulation of oil within the merged eddy and the fact that this eddy did not move substantially for several months. The observed offshore entrainment of oil toward the LC was successfully hindcast using a particle-tracking model based on geostrophic currents computed from satellite altimetry. This assessment of circulation processes may help to advance numerical circulation modeling efforts in this region of rapid current variability in support of safer deepwater drilling in the northern Gulf.

1. INTRODUCTION

On 20 April 2010, the Macondo oil well experienced a massive blowout, causing the explosion and collapse of the *Deepwater Horizon* (DWH) oil rig, 77 km southeast of the Mississippi River Delta (MRD), Louisiana, in 1667 m of water [*Joye and MacDonald*, 2010] (Figure 1). The oil gushed into the Gulf from 22 April to 15 July, releasing approximately 184.8 million gallons of oil ($\pm 20\%$) [*Crone and Tolstoy*, 2010] to which BP added 1.84 million gallons of dispersants [*British Petroleum*, 2010]. Real-time satellite imagery using visible, IR, and radar measurements were essential for tracking the dispersed surface oil across large areas of the Gulf of Mexico (GoM) as well as the ocean currents impacting its motion.

Surface circulation in the oil spill region can be influenced by cyclonic and anticyclonic eddies (ACs) as well as the Loop Current (LC) features that extend vertically to at least

¹Department of Oceanography and Coastal Sciences/Coastal Studies Institute, Louisiana State University, Baton Rouge, Louisiana, USA.

²Center for Astro dynamics Research, University of Colorado, Boulder, Colorado, USA.

³Horizon Marine, Inc., Marion, Massachusetts, USA.

⁴Rosenstiel School of Marine and Atmospheric Science, University of Miami, Miami, Florida, USA.

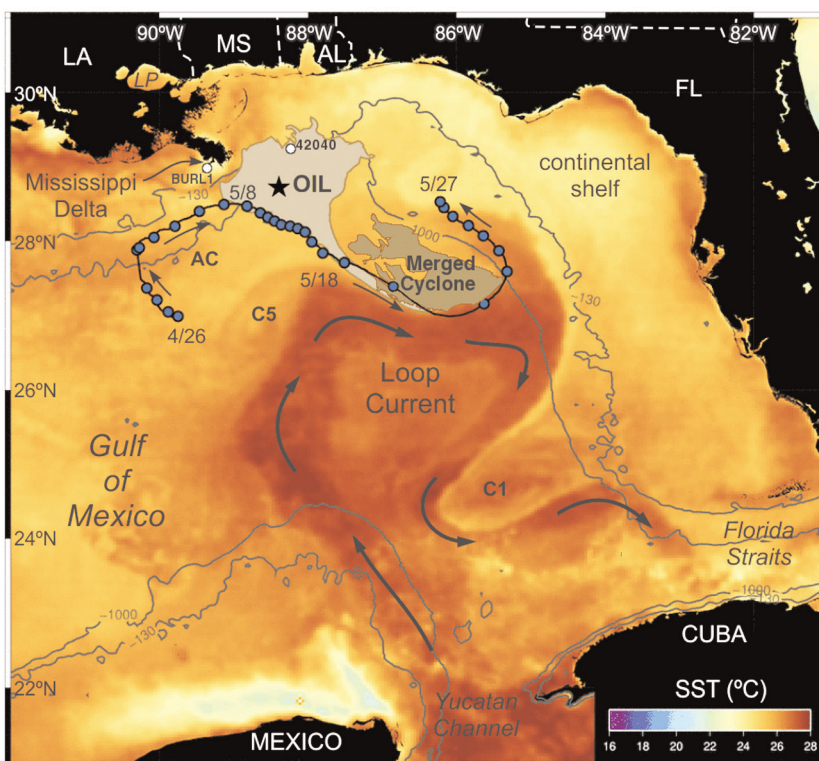


Figure 1. GOES sea surface temperature (SST) composite (17–19 May) showing the Loop Current, the merged cyclone, other Loop Current frontal eddy cyclones (C1, C5), the oil spill location (black star), the wind stations (white dots), and other pertinent landmarks. The oil slick extent (based on synthetic aperture radar (SAR) imagery) on 17 May is depicted with gray, and new oil coverage in the merged cyclone on 18 May is depicted with brown. The track of a drifter is shown from 26 April to 27 May with blue dots ($\sim 1 \text{ day}^{-1}$). The 130 and 1000 m isobaths are indicated with gray lines, and the land is black. The color to temperature (C) conversion is shown in the bottom right corner.

800 m water depth [Vukovich and Maul, 1985]. The LC, an integral component of the Gulf Stream system, enters the GoM through the Yucatan Channel and performs a clockwise retroflection, exiting through the Florida Straits into the North Atlantic Ocean (Figure 1). At the time of the oil spill, the LC's northern margin was at 27°N , about 70 km north of its median position of 26.3°N [Vukovich, 2007]. Cochrane [1972] was the first to describe meanders along the LC margin, features closely associated with cyclonic eddies, later named Loop Current Frontal Eddies (LCFEs) by Frantantoni et al. [1998]. Satellite observations have revealed that two to four LCFEs are typically found moving in the direction of current flow along the LC's outer margin [Vukovich and Maul, 1985; Walker et al., 2003]. Some of these features grow in size as they propagate northward, and the largest features have been observed along the northern margin of the LC [Vukovich and Maul, 1985; Walker et al., 2009].

This study employs satellite measurements, plus in situ current and wind data, to investigate oil motion and the major forcing mechanisms responsible for the observed large-scale

changes in the spatial distribution of the surface oil. An energetic circulation event in May involving the LC and associated cyclonic and ACs is central to this study. This event led to a rapid offshore entrainment of oil into the LC system, tripling oil coverage within 7 days. A 325 km long, surface oil feature (Figure 1) was detected by several satellite sensors, providing researchers with a Lagrangian tracer of circulation, ideal for revealing the presence of eddy circulations. Satellite measurements of sea surface temperature (SST) and sea surface height (SSH), combined with measurements from drifters and acoustic Doppler current profilers (ADCPs), provided the necessary tools to assess and model the evolution of this energetic event, and its impacts on the spread of surface oil across the GoM.

2. DATA AND METHODS

2.1. Surface Oil Detection

Visible band images were available of the spill region twice each day using NASA's Moderate Resolution Imaging

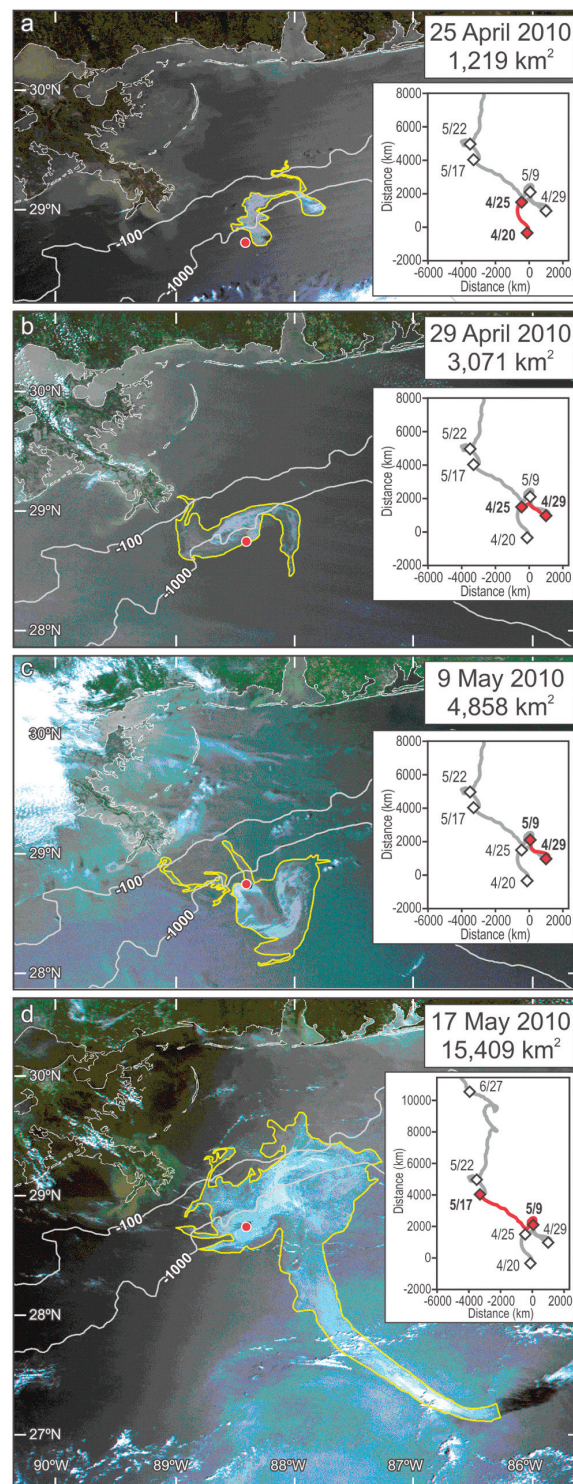
Spectroradiometer (MODIS) sensor (from Terra-1 and Aqua-1 satellites) (Figure 2). The MODIS data were obtained in real-time via antenna at the Louisiana State University Earth Scan Laboratory. Atmospheric Rayleigh scattering corrections, reflectance computations, and registration to 250 m pixels were performed on the Level 1 calibrated data using software of *Gumley et al.* [2003]. “True color” image enhancements were produced using the red (645 nm), green (555 nm), and blue (469 nm) bands (Figure 2). Oil appeared bright tan to white, but only within the sun-glint region of each image, an observation that has been discussed in previous studies [*Adamo et al.*, 2009; *Hu et al.*, 2009]. In early May, synthetic aperture radar (SAR) images became available from several international sensors (CosmoSkymed-1; Radarsat-1, Radarsat-2; ERS-2; Envisat) as a result of the real-time capture and processing capabilities at the University of Miami CStars lab (Figure 3). The SAR system is advantageous for detecting oil since it is not affected by clouds and can be used both day and night [*Brekke and Solberg*, 2005]. SAR sensors measure the reflected pulse of microwave energy from the sea surface and reveal oil (thick or thin) as dark regions, due to oil’s dampening effect on ocean capillary waves, 3–5 cm in length. Low wind areas ($<3 \text{ m s}^{-1}$) can produce false positives; however, offshore wind data revealed sufficiently high wind speeds during acquisition of the SAR images we used (Figure 4a). In several cases of near-contemporaneous SAR and MODIS image acquisitions, the SAR images showed larger areas of oiling, most likely due to (1) its higher sensitivity to oil and (2) the lack of distinct oil signatures in MODIS images away from strong sunglint. Oil coverage was quantified by digitizing the oil features’ margins, based on gradient detection using geographic information system software.

2.2. SST, SSH, Current, and Wind Measurements

We assessed daily changes in the motion of the LC and LCFE cyclones using de-clouded nighttime GOES SST composites [*Walker et al.*, 2003] and near real-time gridded SSH maps interpolated from three altimeters (Envisat, Jason-1, and Jason-2) [*Leben et al.*, 2002; *Walker et al.*, 2005a]. These two types of data, updated daily, provide the best information on LCFEs. Surveillance of these features on a daily basis can

Figure 2. Time-history of the oil spill as shown by the best available MODIS imagery on (a) 25 April, (b) 29 April, (c) 9 May, and (d) 17 May. Digitized plume areas (in km^2) are shown with yellow lines and areas depicted in top right corners. The site of oil release is shown with a red dot. The 100 and 1000 m isobaths are indicated with solid white lines. Progressive wind vector graphics (from 42040) depict wind history between images, using red lines. More detailed wind data is given in Figure 4.

be challenging due to their rapid speeds of $20\text{--}74 \text{ km d}^{-1}$ as well as the frequent cloud cover in the GoM [*Vukovich and Maul*, 1985; *Walker et al.*, 2003, 2009].



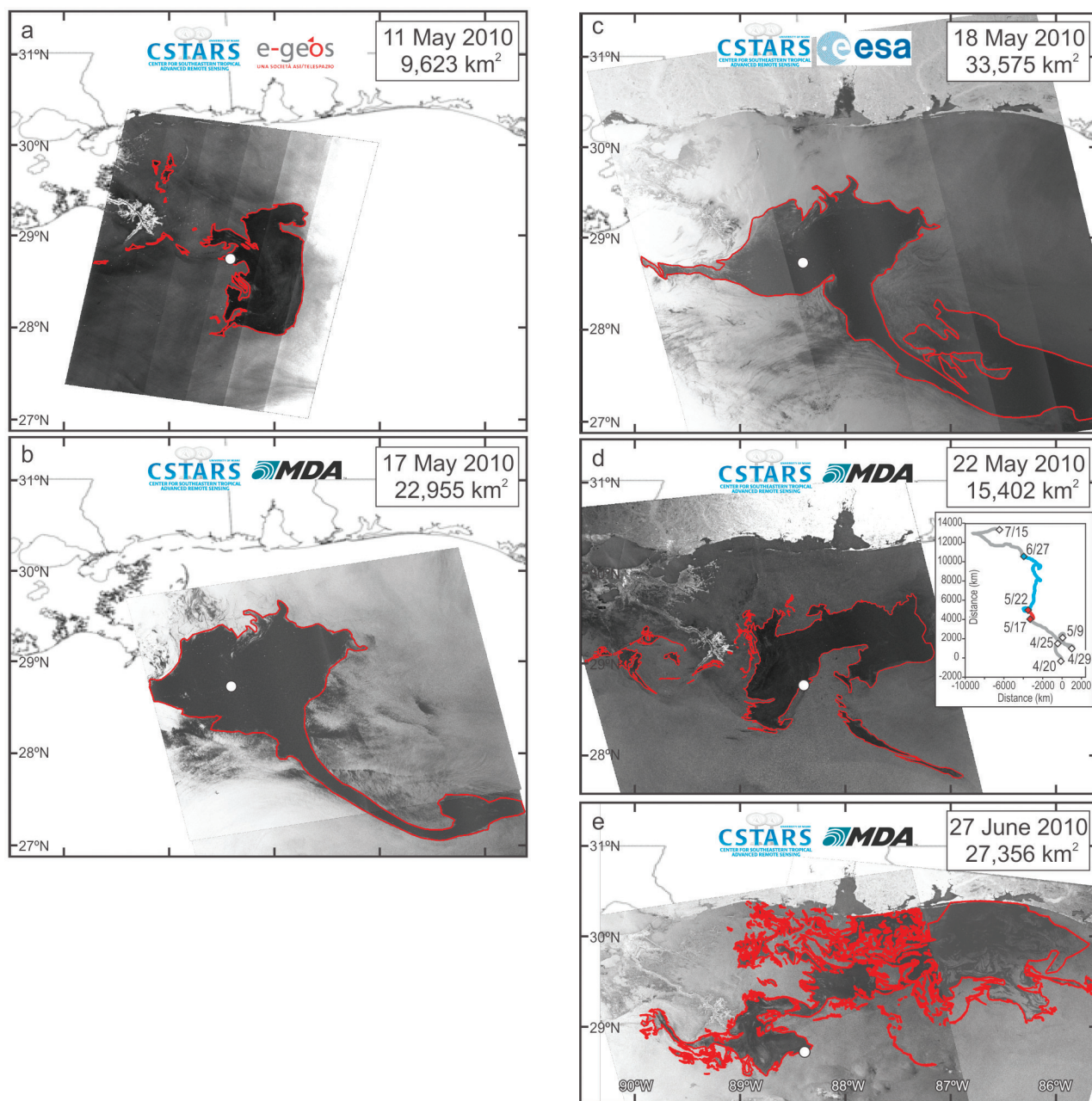


Figure 3. Time-history of the oil spill as shown in best available SAR imagery on (a) 11 May (CosmoSkymed-1), (b) 17 May (Radarsat-2), (c) 18 May (Envisat), (d) 22 May (Radarsat-1), and (e) 27 June (Radarsat-2). The digitized plume areas (km²) are shown with red lines and areas depicted in top right corners. The site of oil release is shown with a white dot. A progressive wind vector graphic (from 42040) in (d) shows wind behavior from 17 May to 22 May (in red) and 22 May to 27 June (in blue).

Surface layer currents were obtained from the 11 m bin of shipboard ADCP data and from motion of a satellite-tracked buoy, drogued at 45 m. Both instruments were deployed and processed by Horizon Marine Inc. ADCP data were collected

from 6 May to 15 July 2010. The drifter was deployed on 26 April and tracked through 27 May 2010. Surface wind measurements were obtained from the nearest CMAN station 42040 (10 m height; 55 km northeast of the spill) and from

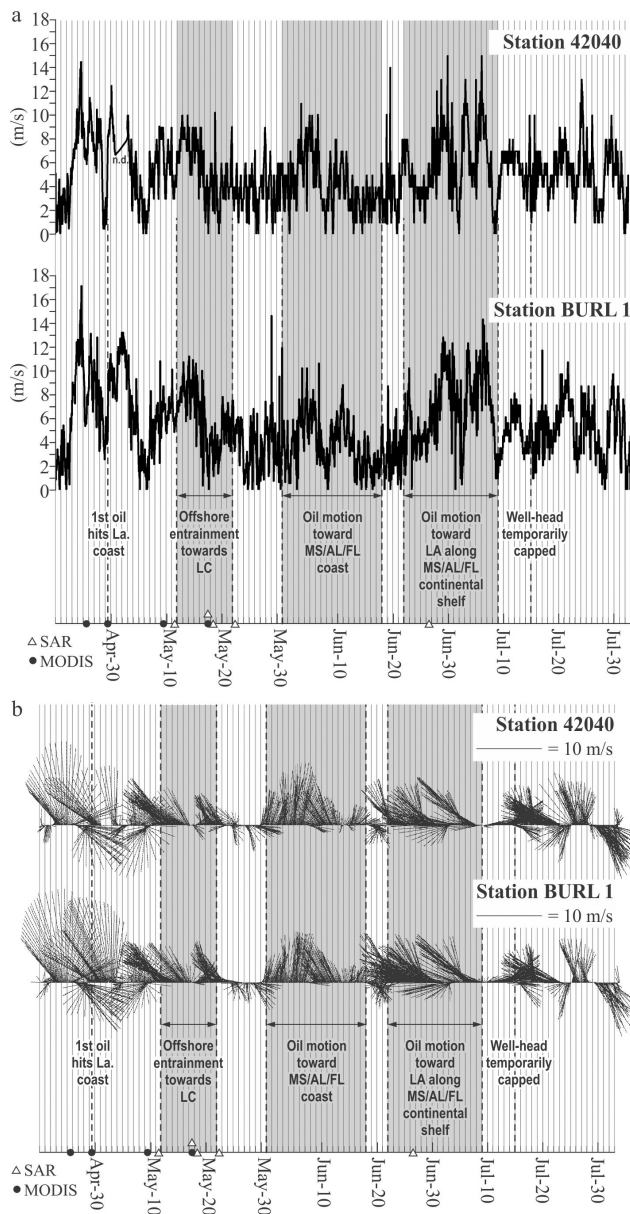


Figure 4. Wind data from stations 42040 and BURL1 from 20 April to 2 August 2010. (a) Wind speeds (smoothed with 5 h running mean) are shown in m s^{-1} with annotation of major events (n.d. indicated missing data), (b) Wind vectors (smoothed with 16 h running mean, subsampled to 5 h) in m s^{-1} with annotation of major events. Vertical lines indicate 00h00 of each day. Vectors extending above the 0 line indicate northward winds. Times of MODIS and SAR image acquisition are indicated with solid black dots and open triangles, respectively.

the MRD Burrwood BURL1 station (33 m height) (see locations in Figure 1). Hourly wind data from 42040 are displayed as progressive vector diagrams in Figures 2 and 3, to

assist in the interpretation of oil motion related to wind forcing. Wind speeds and vectors from both stations are depicted in the two panels of Figure 4. The data in Figure 4 were smoothed to facilitate interpretation. The wind speeds (Figure 4a) were smoothed with a 5 h running mean, and the wind vectors (Figure 4b) were smoothed with a 16 h running mean and subsampled every 5 h. Smoothing was not needed for the data displayed in Figure 5 as the time period was much shorter making the vectors easier to interpret. Times are given in local time (LT) unless stated otherwise.

2.3. Particle Tracking

Daily gridded velocity fields for advecting particles to simulate the spill were obtained from hindcast gridded SSH maps using a geostrophic flow approximation on an f-plane with central finite differencing. The hindcast maps differ from near real-time maps only in the time window applied to the along-track data during the objective analysis procedure [Leben *et al.*, 2002]. The hindcast fields are smoother and presumably more accurate over time than the near real-time fields. Velocities needed to compute the particle paths were interpolated from the gridded velocity fields using a tricubic interpolation scheme [Lekien and Marsden, 2005] in longitude, latitude, and time. The particle positions were integrated through time using a second-order Runge-Kutta

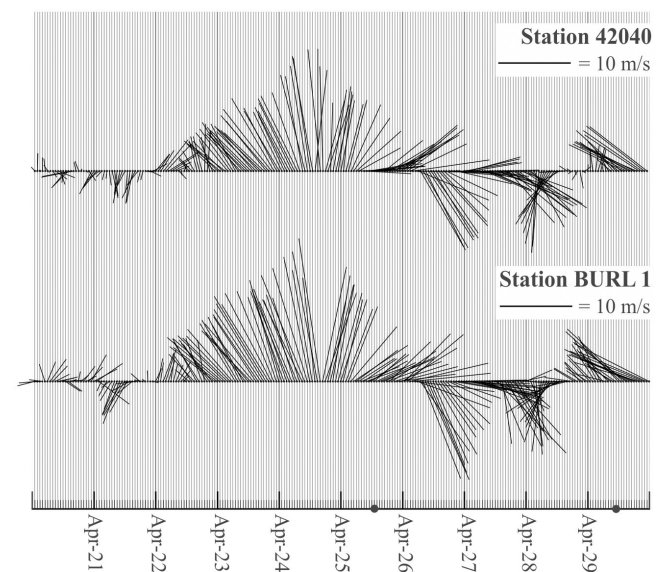


Figure 5. Wind vectors (nonsmoothed) for 20–29 April 2010 from stations 42040 and BURL1. Vectors extending above the 0 line indicate northward winds. Times of MODIS image acquisition are indicated with solid black dots. Vertical lines indicate hours of the day.

method. Twenty-five particles were seeded in a patch $0.2 \times 0.2^\circ$ (0.05° apart) centered on the oil leak every hour over the integration period from 22 April 2010 onward. Integration accuracy was verified by numerical experiments using analytical steady state flow fields. Particles were removed whenever they advected into land-masked grid cells.

It should be noted that this simple model does not consider wind effects, chemical/biological processes, or oil diffusion and degradation. More sophisticated models of the spill using flow fields from data assimilative ocean model simulations with altimeter data assimilation have been developed, which have been used to predict both the surface drift [Liu *et al.*, 2011, this volume(a); Mariano *et al.*, 2011; Huntley *et al.*, this volume] and subsurface drift [Mariano *et al.*, 2011, this volume(a); Weisberg *et al.*, this volume] of the oil. Tactical modeling by NOAA's Office of Response and Restoration during the DWH spill is described in the work of MacFadyen *et al.* [this volume].

3. SURFACE OIL MOTION: 20 APRIL TO 11 MAY

On 25 April, 3 days after the leak began, MODIS imagery revealed surface oil extending 72 km east-northeastward from the leaking wellhead (Figure 2a), net motion that is attributable to a 3 day period of northward winds (Figure 5) and a small AC to the east (Figure 7a). During this period, winds veered slowly from northwestward to northward and northeastward with maximum wind speeds of 20 m s^{-1} at BURL1 on 24 April (Figure 5). By 25 April, the surface oil covered 1219 km^2 most of which was in water depths greater than 500 m (Figure 2a).

The next high-quality clear-sky MODIS image of 29 April showed a spiral-shaped oil feature covering 3071 km^2 and oil within a few kilometers of the MRD, Louisiana (Figure 2b). Over the 4 days between these MODIS images, the western-most oil had to travel at least 50 km to reach the MRD. Wind records at the coast and offshore revealed northeastward, eastward, and southeastward winds ($10\text{--}15 \text{ m s}^{-1}$) from noon of 25 April to noon of 27 April (Figure 5), wind directions that would not favor surface oil motion toward the MRD. However, a lower quality MODIS image of 27 April (1240 CDT) (not shown, but viewable at www.esl.lsu.edu/oilspill/) revealed that the western margin of the oil moved 21 km toward the MRD coastline during this 2 day period of offshore wind forcing. Clearly, forcing mechanisms other than direct wind effects influenced surface oil motion between the leaking wellhead and the MRD between 25 and 27 April.

Winds veered to southward and then southwestward at both stations early on 28 April (Figure 5). At BURL1, winds

continued to veer to northwestward after 1700 CDT on 28 April and intensified to 8 m s^{-1} by noon on 29 April. Offshore at 42040, winds were slower to veer northwestward and only did so at 0700 on 29 April. Based on data from these two stations, wind directions were favorable for oil motion toward the MRD starting early on 28 April. Between 27 and 29 April, the oil moved an additional 30 km toward the MRD, motion that could have resulted from direct wind impacts (with Ekman effects), as the wind blew southward, southwestward, and northwestward (Figure 5).

An additional forcing mechanism influencing circulation in this region is water level slopes, as discussed by Murray [1972] based on time-series measurements northeast of the MRD in 16 m of water. Applying his results to our study, the strong southeastward winds of 26 April (Figure 5) would have caused set-down (lowering) of water levels at the coast and moved surface waters in the offshore direction. With the observed reduction in wind speed late on 26 April, shoreward motion of surface water would be expected. This process may help to explain the motion of oil toward the MRD between 25 and 27 April. The DWH oil first reached the coast late on 29 April and, with several additional days of northwestward wind forcing (29 April to 4 May at BURL1), the oil started to impact the marshes and beaches of eastern Louisiana, north of the MRD (Figure 4b).

The discussion of the relationships between wind forcing and oil motion between 25 and 29 April has highlighted the complexity of surface circulation in the region between the leaking wellhead and the MRD, particularly when wind directions are continuously changing. Previous studies have shown circulation around the MRD to be controlled by wind direction, wind stress [Cochrane and Kelley, 1986; Schroeder *et al.*, 1987; Walker *et al.*, 2005b], and coastal water level slopes [Murray, 1972; Walker *et al.*, 1996]. In addition, large counterclockwise gyres develop on both continental shelf regions, east and west of the MRD with prolonged westward wind forcing [Cochrane and Kelly, 1986; Schroeder *et al.*, 1987]. Westward flow is commonly observed on the continental shelf south of the MRD when winds blow westward [Hitchcock *et al.*, 1997; Walker *et al.*, 2005b]. The western limb of the continental shelf gyre, east of the MRD, may have provided another control on circulation between the leaking wellhead and coastal regions east of the delta, inhibiting northward flow of oil when established.

The MODIS image of 9 May revealed that most of the oil was in water deeper than the leaking wellhead, although two long filaments of oil extended westward and northwestward from the oil spill to the 100 m isobath (Figure 2c). The 11 May SAR image (Figure 3a) revealed more oil in shallower

water than did the MODIS image 2 days earlier. Net wind flow from 20 April to 9 May was mainly northwestward, but changed to southward on 8 May, the day before MODIS image acquisition (Figure 4b). Despite the wind conditions that favored shoreward transport, the large mass of oil remained far offshore, suggesting that deepwater circulation was mainly responsible for the observed oil distribution on 9 and 11 May.

4. OFFSHORE OIL ENTRAINMENT EVENT

On 11 May, SAR imagery revealed a 9623 km² oil slick (Figure 3a), similar in shape to that observed in the 9 May MODIS image (Figure 2c), but covering about twice the area. Oil patches were also detected with SAR in shallow water east and west of the MRD. The main slick extended eastward past 88°W and southward to 28°N. On 17 May, after a 6 day hiatus in data, both MODIS and SAR images revealed a prominent 325 km long and 10–20 km wide oil feature, extending southeastward toward the LC, from a region just east of the oil spill (Figures 2d, 3b). This offshore directed flow occurred in opposition to prevailing northwestward wind forcing of moderate intensity (4–9 m s⁻¹) (Figures 4a, 4b). The oil feature north of the leak had grown in area extending to, and in some places beyond, the 100 m isobath onto the continental shelf, east of the MRD. This northward spread was consistent with the prevailing northwestward winds between 9 and 17 May (Figures 2d, 3a–3c). MODIS images revealed growth in the total oiled area from 4858 to 15,409 km² over 8 days (9 to 17 May) (Figures 2c, 2d) whereas SAR images revealed growth from 9623 to 33,575 km² over 7 days (11 to 18 May) (Figures 3a, 3c).

An AC, cyclonic eddies along the LC margin, and a LC meander were responsible for the large-scale offshore advection of oil that occurred between 11 and 17 May (Figures 1, 6). The AC was apparent on 2 May as a +5 cm region in SSH data, and its clockwise circulation was revealed by the track of the drifting buoy, deployed along its southern margin on 26 April (Figure 6e). The drifter moved along the western and northern margin of the AC in late April and early May. Between 2 and 18 May, three cyclones (C2, C3, C4) flanking the northwest and north margins of the LC merged to form one very large cyclone (280 × 130 km) (Figures 6a–6h). These measurements were based on the –15 cm SSH contour of 18 May (Figures 6d, 6h). The counterclockwise circulation associated with the merged cyclonic eddy (MC) would have encompassed a larger region. This is the first time that a coalescence of three cyclones along the LC margin has been documented. The evolution of this MC appeared to proceed in two main stages, the first stage in-

involved merger of C4 and C3 (the western cyclonic eddies), and the second stage involved the coalescence of C3/4 with C2. Both stages of the merging process resulted in an increase in area and intensity based on the SSH measurements.

Figure 6 presents SST data (a–d), SSH data (e–h), and modeled oil motion (i–l) on 4 days (2, 8, 13, and 18 May) as a representation of this event. In addition, negative SSH contours (low SSH) have been superimposed on SST panels, to facilitate interpretation of the events. On 2 May, the three cyclones involved in the merger (C4, C3, C2) were clearly apparent in the SSH data along the northwestern and northern LC front, with minimum SSH values of –15 cm in each (Figures 6a, 6e). The SST data revealed two cyclones, C4 and C2 (Figure 6a), as they entrained warm LC water in a counterclockwise arc away from the LC. LCFEs, and other GoM cyclones, do not usually exhibit distinct cool cores at the surface, only at 50–60 m and below [Vukovich and Maul, 1985]. However, the LCFEs are often detectable in SST data by the counterclockwise entrainment of warm water away from the LC margin, as was observable for C2 and C4 (Figure 6a). We postulate that since C3 did not exhibit a clear SST signal, it did not influence surface circulation at the LC margin.

The SST and SSH data reveal very different properties of circulation. The SST data is in the form of a raster image that reveals synoptic regional coverage of surface temperature, usually representative of the surface mixed layer [Robinson, 2004]. It is used in this study to reveal locations of SST frontal zones and warm filaments that reveal both cyclonic and AC circulations. Lewis and Kirwan [1985] studied the merger of anticyclones in the western GoM using SST data to identify warm filaments as indicators of eddy flows. Hooker and Brown [1996] used SST data to study the coalescence of three eddies in the Brazil Current. The SSH data is not a raster image, but estimated from measurement along satellite ground tracks that are interpolated to a regular grid over both space and time. The SSH signal is an integration of the density field over the entire water column including any barotropic signals and is dominated by the mesoscale eddy signal in the Gulf [Leben et al., 2002]. In Figures 6a–6h near real-time SSH maps are shown, based on weighted averaging of the multisatellite sampling using only past data with the heaviest weighting on the analysis date. The cyclonic eddies have been labeled based on the SSH contours to simplify the discussion of the merging events.

On 2 May (Figure 6a), the two warm filaments along the northern margin of the LC better revealed the location of the LCFEs. The –15 cm SSH contours are offset from the SST patterns on 2 May as a result of the difference in the measurements, as explained previously. The warm curved

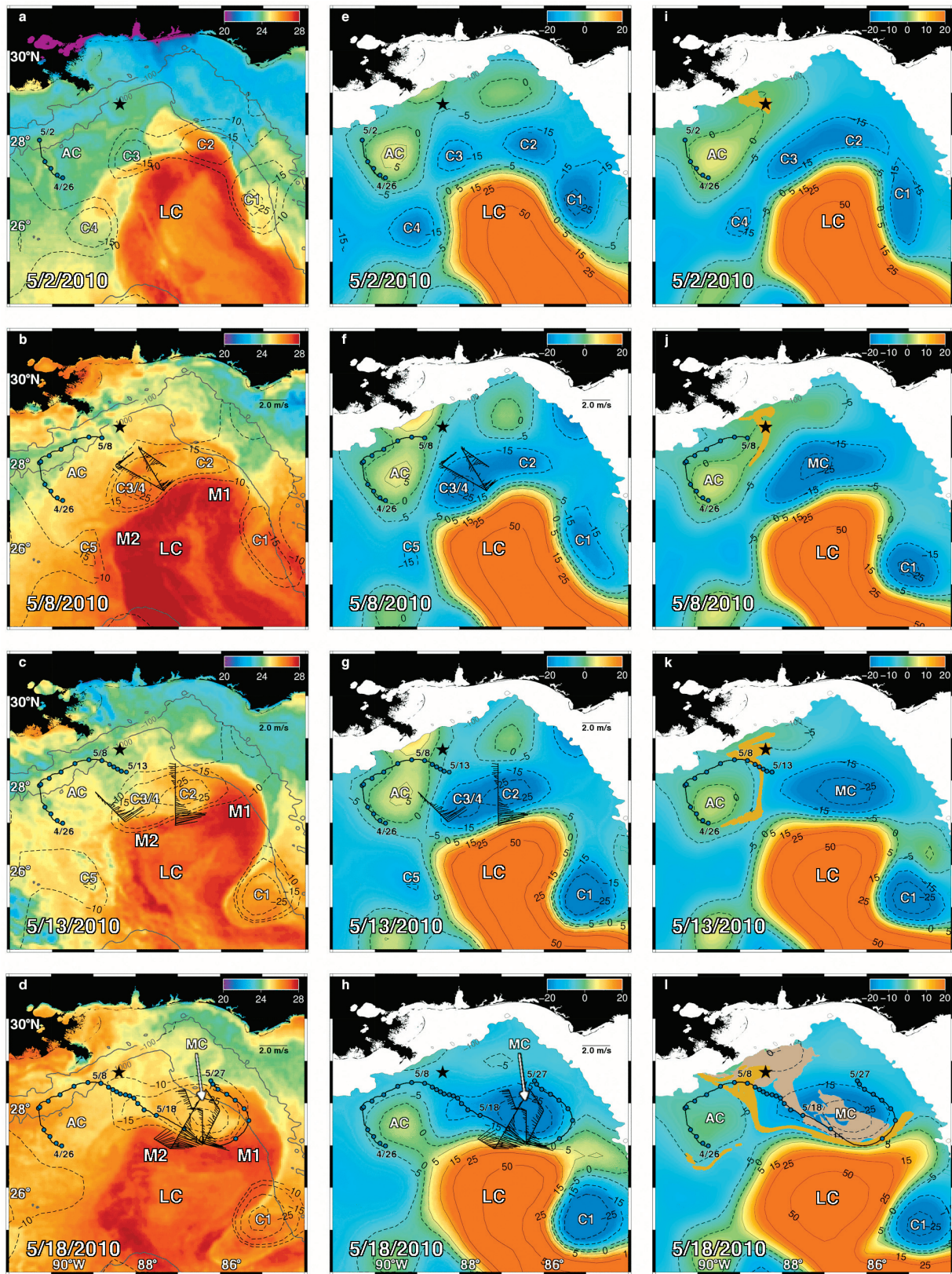


Figure 6

filament on the northwest LC margin is interpreted as C4, having moved recently eastward. C2 corresponded generally to the warm filament on the northeast margin of the LC. As mentioned earlier, C3 had no distinct SST signature. Between 2 and 8 May, C4 moved eastward toward C3 and by 8 May (Figures 6b, 6f), a larger and more intense cyclonic circulation was apparent in the SSH data. The minimum SSH value decreased from -15 cm on 2 May in C3 to -25 cm on 8 May in C3, a change that demonstrates that C4 had merged with C3. An animation of daily de-clouded SST images best reveals the eastward motion of C4 toward C3, further documenting the merger of C4 with C3 by 8 May (SST/SSH Frontal Eddies April 20 to May 31 accessible at <http://www.esl.lsu.edu/oilspill/>). In addition, the -15 cm contour north of the LC increased in area and elongated, encompassing C4, C3, and C2. Five days later on 13 May, further intensification of cyclonic circulation was indicated within C2 (SSH change from -15 to -25 cm) and C3/4 and C2 had moved closer together (Figures 6c, 6g). We suggest that this indicated the beginning of the merging of C3/4 with C2. The imagery of 15 May (not shown) shows further intensification (SSH reduced to -35 cm) and only one center which moved eastward to 86.5°W . An almost identical SSH pattern was observed on 18 May (Figures 6d, 6h). The merger of C3/4 with C2 appeared complete within the 15–18 May time frame, as a more circular and more intense MC was detected in both SSH and SST data (Figures 6d, 6h). The center of the MC on 18 May was at 86.5°W and 27.7°N . The MC maintained its core intensity of -35 cm until 23 May when a reduction to -30 cm was observed (SSH animation is viewable at <http://www.esl.lsu.edu/oilspill/>).

Current measurements from a satellite-tracked drifter and from ADCP crossings of the LC support the satellite-based assessment of circulation. The drifter (drogued at 45 m) was released on 26 April southwest of the oil spill. It initially moved northwestward, then northeastward influenced by the clockwise flow of an AC (Figures 1, 6f). On 8 May, it changed direction to southeastward as it entered a region of

offshore-directed flow, between the AC and counterclockwise flow of the MC (Figure 6g). It moved slowly between 8 and 13 May and then more rapidly as it approached the western margin of the MC. Its entire track is best viewed on 18 May (Figures 1, 6d, 6h). The drifter followed the western margin of the oil slick averaging 0.3 m s^{-1} from 8 to 17 May (Figure 1). It crossed the oil slick on 18 May and accelerated to a maximum speed of 1.82 m s^{-1} on 19 May as it encountered the frontal zone between the LC meander (M2) and the MC (Figures 1, 6d, 6h). The research ship acquiring ADCP data transited the elongated oil feature several times from 15 to 18 May and the log book entry on 17 May 13:45 reported that they were “inside the large 4 x 10 mile oil slick, lat $27^{\circ} 22.20\text{N}$, long $87^{\circ} 17.45\text{W}$ ”. The drifter was entrained around the eastern margin of the MC and departed from the north margin of the MC on 27 May (Figures 6d, 6h), when it stopped reporting.

The ADCP current vector data (from 11 m bin) collected on 8, 12–13, and 18–19 May are superimposed on the respective SST and SSH data panels (Figures 6b–6d, 6f–6h). On 8 May, the vectors confirmed a cyclonic circulation corresponding to the merged and intensified C3/4 (Figures 6b, 6f). On 13 May, currents for 12 and 13 May are superimposed. The 12 May ADCP line crossed the center of C2, confirming its cyclonic circulation. ADCP currents exhibited little flow within the -25 cm central region, westward flow north of its center, and eastward flow in the frontal zone associated with the LC (Figures 6c, 6g). The ADCP line of 13 May was influenced by the LC meander (M2) which was moving rapidly northward. Measured currents along this line were strongest on the northwest margin of the LC, which correlated closely with the SST patterns (Figure 6c), but not as well with the SSH data (Figures 6c, 6g). The SSH measurements along the south side of this transect had not been updated with new data to reflect recent northward motion of M2. On 18 May (Figures 6d, 6h), several ADCP transects are shown that transect the MC. The current patterns confirm the large MC and its cyclonic circulation. Strongest currents

Figure 6. (opposite) Time-history of circulation and oil motion on 2, 8, 13, and 18 May 2010 as revealed by (a–d) GOES SST data ($^{\circ}\text{C}$) (e–h) real-time sea surface height (SSH) data (cm), and (i–l) tracking of oil particles using hindcast SSH data. SSH data displayed on (a)–(d) are identical to those of (e)–(h) but include only the negative contours of -10 , -15 , -25 , and -35 cm. SSH data on (e)–(l) include positive contours of 5, 15, 25, and 50; negative contours of -25 , -15 , -5 , and a zero line. Bathymetry lines (100 and 1000 m) are superimposed on the SST data. In all panels, solid lines depict high SSH, i.e., the LC and anticyclonic eddies (ACs); and dashed lines depict low SSH, i.e., cyclonic eddies (C). Daily drifter positions (~ 1100 UTC) are depicted on all panels with blue dots. acoustic Doppler current profiler currents from 8 May are superimposed on the 8 May images (b, f), 12–13 May currents are superimposed on the 13 May images (c, g), and 18–19 May currents are superimposed on the 18 May images (d, h). Current vectors are shown with black lines and extend outward from the linear ship tracks. A vector scale is provided. Cyclones are annotated as C1–C5 and LC meanders as M1 and M2. The merged cyclone is labeled MC. Modeled oil particle locations are colored orange (i–l). In (l) the oil slick from the 18 May SAR image (Figure 3c) is depicted in a beige color. The site of oil release is shown with a black star. Legends are shown in upper right corners and dates in lower left corners.

were measured along the LC margin with maxima of 2.25 m s^{-1} on 12 May and 2.03 m s^{-1} on 19 May, both within the frontal zone separating the LC and the MC, between 86.4°W and 87.1°W (Figures 6c, 6d, 6g, 6h). These observations coincided closely with the location of maximum currents along the drifter track on 19 May (Figures 6d, 6h).

The 18 May SAR image revealed that oil mainly accumulated in the southern and central regions of the MC (Figures 1, 6l). The oil entrainment event was short-lived as imagery demonstrated a severing of the oil filament by 22 May, and reconnection was not observed (Figure 3d). The circulation system that favored offshore entrainment of the surface oil toward the LC was likely disrupted by southward movement of the AC and eastward movement of the MC. In addition, the flow of oil was reported to have been reduced at the wellhead on 17 May due to initiation of subsea dispersant usage as well as collection of oil with a riser insertion tube [McNutt, 2010].

A particle-tracking model, based on upper ocean geostrophic currents, computed from the daily hindcast SSH fields, reproduced surface oil motion toward the LC (Figures 6i–6l). The model revealed southward motion of oil from 2 to 8 May, following the eastern margin of the weak AC (AC core is yellow, Figures 6i, 6j). On 13 May, the oil turned westward apparently still influenced by the AC circulation (Figure 6k). On 14 May, the mass of oil turned to the east, as it encountered the northern margin of the LC near M2, and it continued on this course through 18 May (Figure 6l). The tracking model results corresponded fairly closely with the track of the drifter (although the drifter lagged the modeled oil) until the drifter escaped the MC's influence on 27 May. The modeled oil circled counterclockwise around the outer margin of the MC (see CCAR model animation at <http://www.esl.lsu.edu/oilspill/>). In contrast, the SAR image of 18 May indicated most of the oil accumulated in the central and southern regions of the large MC. The wind on 17–18 May was relatively weak, and thus not considered a major control on oil motion in this offshore region.

5. OIL MOTION, WINDS, AND CURRENTS: JUNE/JULY/AUGUST

This dynamic eddy merger event was followed by the detachment of the northern portion of the LC as a large AC on 14 June (Figure 7b). This detachment date is based on the tracking and breaking of the 17 cm LC SSH contour as discussed by *Leben* [2005]. By definition, a “detached” eddy eventually reattaches to the LC, whereas a “separated” eddy refers to the ultimate detachment or separation of an eddy. The newly detached AC, named Eddy Franklin by Horizon Marine Inc., had dimensions of $300 \times 300 \text{ km}$,

typical of recently detached warm eddies [*Leben*, 2005; *Vukovich*, 2007]. After separation, ACs usually move slowly toward the western Gulf [*Cochrane*, 1972; *Vukovich*, 2007]. However, this detached AC and the MC that remained on its northern margin exhibited little westward motion allowing the LC to recapture it on 31 July (Figure 7c). The MC became a blocking cyclone, trapped by shoaling topography of the west Florida escarpment, which limited its eastward and southward motion (Figures 7c, 7d, see 1000 m isobath). The 18 August image (Figure 7d) revealed another AC detachment event. At this time, the MC was larger than the AC. *Hamilton et al.* [this volume] studied the motion of drifters in relation to SSH and suggest that detachment and reattachment occurred as many as five times between mid-June and September with final separation of Eddy Franklin occurring on 29 September according to an analysis of the hindcast SSH maps. *Liu et al.* [this volume(b)] also provide a description of circulation events in the LC system throughout this time period, by computing geostrophic currents from the Archiving, Validation, and Interpretation of Satellite Oceanographic data SSH anomaly data with validation from drifting buoys.

By 27 June, SAR imagery revealed a massive area of oil/dispersant covering $\sim 27,356 \text{ km}^2$ of the continental shelf of the northeast GoM (Figure 3e). Northward oil motion was clearly forced by a 2 week period during which winds blew northward and northeastward (Figures 3d, 4b). Although the most prevalent wind direction in the northeast GoM in spring and summer is westward, this pattern is interrupted for several weeks each summer by northward and northeastward winds [*Cochrane and Kelly*, 1986; *Walker et al.*, 2005a; *Morey et al.*, 2003] as was observed in June 2010 (Figure 4b). Westward winds returned on 22 June, initiating a westward inner shelf flow of oil toward Louisiana. Thereafter, winds blew mainly to the west resulting in westward motion of oil until 9 July. The oil distribution maps provided in the work of *Liu et al.* [this volume(b)] show an accumulation of oil along the eastern Louisiana coast between 25 June and 9 July, as a result of this major and prolonged wind direction change from eastward to westward. The wellhead was successfully capped on 15 July, and confirmation of cementing success was obtained on 9 August [*British Petroleum*, 2010].

6. SUMMARY AND CONCLUSIONS

We have tracked large-scale changes in the DWH surface oil slicks from 25 April to 27 June 2010 and discussed major causal mechanisms for the observed motion, including direct and indirect wind effects and deepwater currents. Motion of oil toward coastal regions resulted mainly from direct wind

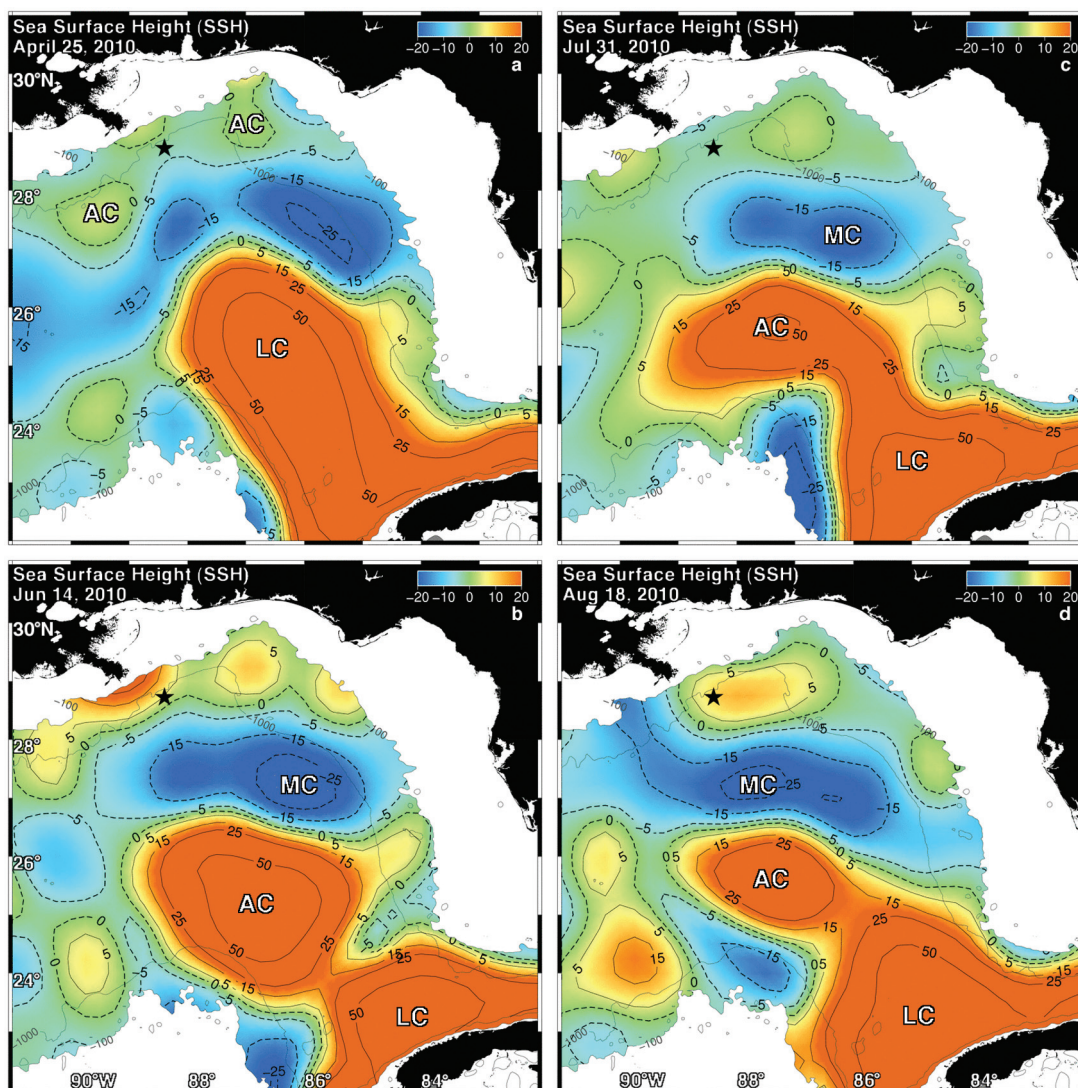


Figure 7. Time history of near real-time SSH (cm) showing (a) 25 April showing the AC east of the leaking wellhead, (b) June 14 showing the initial detachment of the large warm AC, (c) 31 July showing LC re-attachment to the AC, and (d) 18 August detachment of the AC from LC. The MC remained on the northern margin of the AC upon detachment from the LC and did not spin down within the period of study. Final separation of Eddy Franklin occurred on 29 September according to an analysis of the hindcast data [Hamilton *et al.*, this volume].

effects when wind direction was sustained for several days to weeks. However, motions around the MRD were complex and related to additional forcing mechanisms, such as sea level slopes. Deepwater currents and their impacts on oil motion were investigated by analyzing satellite SST and SSH data in tandem with contemporaneous in situ current data. The most prominent offshore entrainment event of surface oil involved the LC that intruded relatively far north in the Gulf. An AC, three cyclonic eddies, and a LC meander were responsible for the large-scale offshore advection of oil

southeastward toward the LC that resulted in an elongated (325 km) and narrow (10–20 km) oil slick by 17 May. SAR images revealed a tripling of the surface oil slick area over 7 days (from 11 to 18 May) with a maximum surface area of 33,575 km² on 18 May. A satellite-tracked drifter (drogued at 45 m) and ADCP currents (at 11 m) revealed high velocity flow of 1.8–2.25 m s⁻¹ within the LC/MC frontal zone between 12 and 19 May.

We documented a merging of three cyclonic eddies along the LC margin, during the offshore entrainment event. This

merging event appeared to occur in two main phases: the westernmost cyclonic eddies merged first, and then, the product of their merger moved eastward to merge with the eastern cyclonic eddy. The final merged cyclone was larger and more intense than the cyclonic eddies that formed it. These observations agree with the modeling results of *Waugh* [1992] concerning symmetric vortex merging, as his 2VD model predicts that the merging process forms larger scales by about 50%. The merged cyclone measured 130 km (north-south) and 280 km (west-east) on 18 May. LC frontal eddy cyclones of similar size have been observed north of the LC before the detachment of large warm core anticyclones [*Hamilton et al.*, this volume], such as Eddy Franklin in this study. It is likely that eddy merging events, similar to the one that impacted the DWH oil spill, are not uncommon along the LC front and large merged cyclones play an important role in the separation of LC anticyclones.

Of considerable interest is the fact that most of the oil accumulated within the large cyclone rather than moving along the LC frontal zone to the southeast toward the Florida Straits. This accumulation of oil and the fact that the large MC remained nearly stationary for several months reduced the threat of oil exposure in the Florida Keys and along the U.S. eastern seaboard. A geostrophic particle-tracking model, based on the hindcast SSH data, successfully re-created the flow regime toward the LC and between the LC and the MC. The modeled oil, however, did not accumulate in the cyclonic eddy but was entrained along the outer margin of the cyclonic circulation. The satellite-tracked drifter, even though drogued at 45 m, exhibited a similar path to the modeled oil until 27 May, when it stopped reporting. *Wade et al.* [this volume] measured oil concentrations in the vicinity of the LC and associated eddies after this event and found highest concentrations in the region of the large MC, in general agreement with the SAR image of 18 May.

Prior research has shown that the LC and eddies (cyclones, anticyclones) that often impinge against the shelf break east of the MRD can entrain Mississippi River water, sediments, nutrients, and pollutants into deep water and subsequent entrainment by the LC can carry river water to the Florida Straits and beyond [*Hu et al.*, 2005; *Walker et al.*, 2005b; *Schiller et al.*, 2011]. The coalescence of LCFEs to form larger and more intense cyclonic features may enhance this offshore entrainment process. Our observations of oil motion, however, suggest that the large cyclones may capture a significant amount of river water, potentially reducing the transport to the Florida Straits along the LC front. Additional observational research and modeling of LC frontal cyclonic eddy circulation processes along the LC margin are warranted based on these new findings.

Acknowledgments. Funding for research and data collection was provided by NASA NNA07CN12A (Applied Sciences Program), as well as from BP to Horizon Marine Inc. and to Louisiana State University (LSU). The Shell Oil Company is also acknowledged for partial funding of LSU research. Support for Robert Leben and Nicholas Hoffmann came from BOEMRE Contracts M08PC20043 and M10PC00112 to Science Applications International Corporation, and the NASA Ocean Surface Topography Mission Science Team Grant NNX08AR60G is also gratefully acknowledged for funding. These findings do not necessarily represent the opinions of BOEMRE. Appreciation is extended to the anonymous reviewers for their insightful comments on this manuscript.

REFERENCES

- Adamo, M., G. DeCarolis, V. DePasquale, and G. Pasquariello (2009), Detection and tracking of oil slicks on sun-glittered visible and near infrared satellite imagery, *Int. J. Remote Sens.*, *30*, 6403–6427.
- Brekke, C., and H. Solberg (2005), Oil spill detection by satellite remote sensing, *Remote Sens. Environ.*, *95*, 1–13.
- British Petroleum (2010), Sustainability Review 2010 Report, BP Global, London, U. K. [Available at <http://www.bp.com/sustainability> or http://www.bp.com/assets/bp_internet/globalbp/STAGING/global_assets/e_s_assets/e_s_assets_2010/downloads_pdfs/bp_sustainability_review_2010.pdf.]
- Cochrane, J. (1972), Separation of an anticyclone and subsequent developments in the Loop Current (1969), in *Contributions on the Physical Oceanography of the Gulf of Mexico*, edited by L. Capuro and J. Reid, pp. 91–106, Gulf, Houston, Tex.
- Cochrane, J., and F. Kelly (1986), Low-frequency circulation on the Texas-Louisiana continental shelf, *J. Geophys. Res.*, *91*, 10,645–10,659.
- Crone, T., and M. Tolstoy (2010), Magnitude of the 2010 Gulf of Mexico oil leak, *Science*, *330*(6004), 634, doi:10.1126/science.1195840.
- Fratantoni, P. S., T. N. Lee, G. P. Podesta, and F. Muller-Karger (1998), The influence of Loop Current perturbations on the formation and evolution of Tortugas eddies in the southern Straits of Florida, *J. Geophys. Res.*, *103*(C11), 24,759–24,779.
- Gumley, L., J. Desclotres, and J. Schmaltz (2003), Creating repro-jected true color MODIS images: A tutorial, Space Sci. and Eng. Cent., Univ. of Wis., Madison. [Available at <http://cimss.ssec.wisc.edu/imapp/>.]
- Hamilton, P., K. A. Donohue, R. R. Leben, A. Lugo-Fernández, and R. E. Green (2011), Loop Current observations during spring and summer of 2010: Description and historical perspective, in *Monitoring and Modeling the Deepwater Horizon Oil Spill: A Record-Breaking Enterprise*, *Geophys. Monogr. Ser.*, doi:10.1029/2011GM001116, this volume.
- Hitchcock, G. L., W. J. Wiseman Jr., W. C. Boicourt, A. J. Mariano, N. Walker, T. A. Nelsen, and E. Ryan (1997), Property fields in an effluent plume of the Mississippi River, *J. Mar. Syst.*, *12*, 109–126.

- Hooker, S. B., and J. W. Brown (1996), Dipole rings and vortex interactions of the Brazil current, *IEEE Trans. Geosci. Remote Sens.*, *34*, 1323–1330.
- Hu, C., J. R. Nelson, E. Johns, Z. Chen, R. H. Weisberg, and F. E. Müller-Karger (2005), Mississippi River water in the Florida Straits and in the Gulf Stream off Georgia in summer 2004, *Geophys. Res. Lett.*, *32*, L14606, doi:10.1029/2005GL022942.
- Hu, C., X. Li, W. G. Pichel, and F. E. Müller-Karger (2009), Detection of natural oil slicks in the NW Gulf of Mexico using MODIS imagery, *Geophys. Res. Lett.*, *36*, L01604, doi:10.1029/2008GL036119.
- Huntley, H. S., B. L. Lipphardt Jr., and A. D. Kirwan Jr. (2011), Surface drift predictions of the *Deepwater Horizon* spill: The Lagrangian perspective, in *Monitoring and Modeling the Deepwater Horizon Oil Spill: A Record-Breaking Enterprise*, *Geophys. Monogr. Ser.*, doi:10.1029/2011GM001097, this volume.
- Joye, S. and I. Macdonald (2010), Offshore oceanic impacts from the BP oil spill, *Nat. Geosci.*, *3*, 446.
- Leben, R. (2005), Altimeter-derived Loop Current metrics, in *Circulation in the Gulf of Mexico: Observations and Models*, *Geophys. Monogr. Ser.*, vol. 161, edited by W. Sturges, and A. Lugo-Fernandez, pp. 181–201, AGU, Washington, D. C.
- Leben, R., G. Born, and B. Engebrecht (2002), Operational altimeter data processing for mesoscale monitoring, *Mar. Geod.*, *25*, 3–18.
- Lekien, F., and J. Marsden (2005), Tricubic interpolation in three dimensions, *Int. J. Numer. Methods Eng.*, *63*, 455–471.
- Lewis, J. K., and A. D. Kirwan Jr. (1985), Some observations of ring topography and ring-ring interactions in the Gulf of Mexico, *J. Geophys. Res.*, *90*, 9017–9028.
- Liu, Y., R. H. Weisberg, C. Hu, and L. Zheng (2011), Tracking the *Deepwater Horizon* oil spill: A modeling perspective, *Eos Trans. AGU*, *92*(6), 45, doi:10.1029/2011EO060001.
- Liu, Y., R. H. Weisberg, C. Hu, and L. Zheng (2011a), Trajectory forecast as a rapid response to the *Deepwater Horizon* oil spill, in *Monitoring and Modeling the Deepwater Horizon Oil Spill: A Record-Breaking Enterprise*, *Geophys. Monogr. Ser.*, doi:10.1029/2011GM001121, this volume.
- Liu, Y., R. H. Weisberg, C. Hu, C. Kovach, and R. Riethmüller (2011b), Evolution of the Loop Current system during the *Deepwater Horizon* oil spill event as observed with drifters and satellites, in *Monitoring and Modeling the Deepwater Horizon Oil Spill: A Record-Breaking Enterprise*, *Geophys. Monogr. Ser.*, doi:10.1029/2011GM001127, this volume.
- MacFadyen, A., G. Y. Watabayashi, C. H. Barker, and C. J. Beegle-Krause (2011), Tactical modeling of surface oil transport during the *Deepwater Horizon* spill response, in *Monitoring and Modeling the Deepwater Horizon Oil Spill: A Record-Breaking Enterprise*, *Geophys. Monogr. Ser.*, doi:10.1029/2011GM001128, this volume.
- Mariano, A. J., V. H. Kourafalou, A. Srinivasan, H. Kang, G. R. Halliwell, E. H. Ryan, and M. Roffer (2011), On the modeling of the 2010 Gulf of Mexico Oil Spill, *Dyn. Atmos. Oceans*, *52*(1–2), 322–340.
- McNutt, M. (2010), Summary preliminary report from the Flow Rate Technical Group, 3 pp. U.S. Geol. Surv., Reston, Va. [Available at http://www.usgs.gov/foia/FRTG_emails/06-02-2010...FRTG%20Preliminary%20Report%20and%20Transcript.pdf.]
- Morey, S. L., P. J. Martin, J. J. O'Brien, A. A. Wallcraft, and J. Zavala-Hidalgo (2003), Export pathways for river discharged fresh water in the northern Gulf of Mexico, *J. Geophys. Res.*, *108*(C10), 3303, doi:10.1029/2002JC001674.
- Murray, S. (1972), Observations on wind, tidal and density-driven currents in the vicinity of the Mississippi River delta, in *Shelf-Sediment Transport*, edited by D. Swift, D. Duane, and O. Pilkey, pp. 127–142, Dowden Hutchinson Ross, Stroudsburg, Pa.
- Robinson, I. S. (2004), *Measuring the Oceans from Space*, Springer, New York.
- Schiller, R. V., V. H. Kourafalou, P. Hogan, and N. D. Walker (2011), The dynamics of the Mississippi River plume: Impact of topography, wind and offshore forcing on the fate of plume waters, *J. Geophys. Res.*, *116*, C06029, doi:10.1029/2010JC006883.
- Schroeder, W., S. Dinnel, W. Wiseman, and W. Merrell (1987), Circulation patterns inferred from the movement of detached buoys in the eastern Gulf of Mexico, *Cont. Shelf Res.*, *7*, 883–894.
- Vukovich, F. (2007), Climatology of ocean features in the Gulf of Mexico using satellite remote sensing data, *J. Phys. Oceanogr.*, *37*, 689–707, doi:10.1175/JPO2989.1.
- Vukovich, F., and G. Maul (1985), Cyclonic eddies in the eastern Gulf of Mexico, *J. Phys. Oceanogr.*, *15*, 105–117.
- Wade, T. L., S. T. Sweet, J. N. Walpert, J. L. Sericano, J. J. Singer, and N. L. Guinasso Jr. (2011), Evaluation of possible inputs of oil from the *Deepwater Horizon* spill to the Loop Current and associated eddies in the Gulf of Mexico, in *Monitoring and Modeling the Deepwater Horizon Oil Spill: A Record-Breaking Enterprise*, *Geophys. Monogr. Ser.*, doi:10.1029/2011GM001095, this volume.
- Walker, N., O. Huh, L. Rouse Jr., and S. Murray (1996), Evolution and structure of a coastal squirt off the Mississippi River delta: Northern Gulf of Mexico, *J. Geophys. Res.*, *101*(C9), 20,643–20,655.
- Walker, N., S. Myint, A. Babin, and A. Haag (2003), Advances in satellite radiometry for the surveillance of surface temperatures, ocean eddies and upwelling processes in the Gulf of Mexico using GOES-8 measurements during summer, *Geophys. Res. Lett.*, *30*(16), 1854, doi:10.1029/2003GL017555.
- Walker, N. D., R. R. Leben, and S. Balasubramanian (2005a), Hurricane-forced upwelling and chlorophyll a enhancement within cold-core cyclones in the Gulf of Mexico, *Geophys. Res. Lett.*, *32*, L18610, doi:10.1029/2005GL023716.
- Walker, N., W. Wiseman, L. Rouse Jr., and A. Babin (2005b), Effects of river discharge, wind stress, and slope eddies on circulation of the Mississippi river plume, Louisiana, *J. Coastal Res.*, *21*, 1228–1244.

- Walker, N., R. Leben, S. Anderson, J. Feeney, P. Coholan, and N. Sharma (2009), Study of Loop Current frontal eddies based on satellite remote sensing and drifter data, *OCS Study MMS 2009-023*, 78 pp., U. S. Dept. of the Inter., Miner. Manage. Serv., Gulf of Mexico OCS Reg., New Orleans, La.
- Waugh, D. W. (1992), The efficiency of symmetric vortex merger, *Phys. Fluids*, 4, 1745–1758.
- Weisberg, R. H., L. Zheng, and Y. Liu (2011), Tracking subsurface oil in the aftermath of the *Deepwater Horizon* well blowout, in *Monitoring and Modeling the Deepwater Horizon Oil Spill: A Record-Breaking Enterprise*, *Geophys. Monogr. Ser.*, doi:10.1029/2011GM001131, this volume.
-
- P. J. Brickley, P. D. Coholan, and N. Sharma, Horizon Marine, Inc., 15 Creek Rd., Marion, MA 02738, USA.
- E. J. D'Sa, C. T. Pilley, V. V. Raghunathan and N. D. Walker, Department of Oceanography and Coastal Sciences/Coastal Studies Institute, Louisiana State University, Baton Rouge, LA 70803, USA. (nwalker@lsu.edu)
- H. C. Graber and R. E. Turner, Rosenstiel School of Marine and Atmospheric Science, 4600 Rickenbacker Causeway, University of Miami, Miami, FL 33145, USA.
- N. G. Hoffmann and R. R. Leben, Center for Astrodynamics Research, University of Colorado, Boulder, CO 80309, USA.